

## Organic Lasers

How to cite:

International Edition: doi.org/10.1002/anie.202008940

German Edition: doi.org/10.1002/ange.202008940

## Experimentally Observed Reverse Intersystem Crossing-Boosted Lasing

Zhonghao Zhou, Chan Qiao, Kang Wang, Lu Wang, Jie Liang, Qian Peng, Zhiyou Wei, Haiyun Dong, Chuang Zhang, Zhigang Shuai, Yongli Yan,\* and Yong Sheng Zhao\*

**Abstract:** Thermally activated delayed-fluorescent (TADF) materials are anticipated to overcome triplet-related losses towards electrically driven organic lasers. Thus far, contributions from triplets to lasing have not yet been experimentally demonstrated owing to the limited knowledge about the excited-state processes. Herein, we experimentally achieve reverse intersystem crossing (RISC)-boosted lasing in organic microspheres with uniformly dispersed TADF emitters. In these materials, triplets are continuously converted to radiative singlets through RISC, giving rise to reduced losses in stimulated emission. The involvement of regenerated singlets in population inversion results in a thermally activated lasing; that is, the lasing intensity increases with increasing temperature, accompanied by accelerated depletion of the excited-state population. Benefiting from the suppression of triplet accumulations by RISC processes, a high-repetition-rate microlaser was achieved.

## Introduction

Organic solid-state lasers, which can generate intense coherent light across the full visible spectrum,<sup>[1]</sup> have captured broad research interest because of their promising applications ranging from sensing to laser displays.<sup>[2]</sup> Attempts to observe electrically driven lasing from organic semiconductor

materials have been widespread but not yet met with success, which is mainly due to the severe optical losses caused by metallic electrodes, charge carriers and triplet excitons.<sup>[3]</sup> Among these challenges, the most difficult impediment towards organic laser diodes is the optical losses related to triplet excitons. Electrically injected charge carriers generally recombine to form radiative singlet and non-radiative triplet excitons in a 1:3 ratio according to spin statistics, which severely limits the internal quantum efficiencies of electrically driven organic lasers.<sup>[1c]</sup> Moreover, the accumulation of long-lived triplet excitons dissipates excitation energy as heat through triplet excited-state absorption (ESA) and exciton annihilation,<sup>[3b,4]</sup> resulting in an extremely high lasing threshold and poor stability of the devices.

Thermally activated delayed fluorescence (TADF) process, featuring a reverse intersystem crossing (RISC) from triplet states to singlet states, is promising for dealing with triplet losses.<sup>[1c]</sup> The RISC process enables upconversion of excited energy from triplet to singlet states at room temperature (RT), which has been widely applied in organic light-emitting diodes to obtain a 100% internal quantum efficiency.<sup>[5]</sup> RISC processes are expected to not only diminish triplet losses by reducing the accumulation of triplets but also provide regenerated singlets for population inversion. Therefore, organic TADF materials with large optical gains are of great interest for their potential in utilizing triplet excitons for lasing. Very recently, amplified spontaneous emission (ASE) was successively demonstrated with organic TADF materials.<sup>[6]</sup> Nevertheless, no explicit contribution from triplet excitons to light amplification has been experimentally observed, which might be attributed to the limited knowledge about the relationships between the fast lasing processes and relatively low RISC processes. Thus far, whether the triplet excitons harvested through RISC processes promote lasing action remains uncertain, which hinders the applications of TADF materials in organic lasers.

Herein, for the first time, we experimentally demonstrate a RISC-boosted lasing in organic microspheres with uniformly distributed TADF emitters, which otherwise cannot be achieved owing to the suppression of delayed fluorescence. TADF molecules with balanced optical gain and triplet-harvesting ability were homogeneously dispersed in self-assembled microspheres, which functioned as high-quality (*Q*) whispering-gallery-mode (WGM)-type resonators. By continuously converting non-radiative triplet excitons to radiative singlet excitons, the RISC process directly contributes to population inversion. Thermally activated lasing was therefore achieved in these microspheres, where RISC

[\*] Z. Zhou, C. Qiao, Dr. K. Wang, J. Liang, Dr. H. Dong, Prof. C. Zhang, Prof. Y. Yan, Prof. Y. S. Zhao  
Key Laboratory of Photochemistry, Institute of Chemistry, Chinese Academy of Sciences  
Beijing 100190 (China)  
E-mail: ylyan@iccas.ac.cn  
yszha@iccas.ac.cn

L. Wang, Prof. Z. Shuai  
Department of Chemistry and MOE Key Laboratory of Organic Optoelectronics and Molecular Engineering, Tsinghua University  
Beijing 100084 (China)

Prof. Q. Peng  
Key Laboratory of Organic Solids and Beijing National Laboratory for Molecular Science, Institute of Chemistry, Chinese Academy of Sciences, Beijing 100190 (China)

Z. Wei  
State Key Laboratory of Molecular Reaction Dynamics, Institute of Chemistry, Chinese Academy of Sciences, Beijing 100190 (China)

Z. Zhou, C. Qiao, J. Liang, Z. Wei, Prof. Y. S. Zhao  
University of Chinese Academy of Sciences, Beijing 100049 (China)

Supporting information and the ORCID identification number(s) for the author(s) of this article can be found under:  
<https://doi.org/10.1002/anie.202008940>

processes played a key role in harvesting triplet excitons and reducing triplet losses. An unusual temperature dependence of the lasing intensity was observed and reasonably ascribed to the well-maintained triplet-harvesting capability due to the uniform dispersion of TADF emitters in the organic microspheres. Benefiting from the management of triplet accumulations by RISC processes, we realized lasing of these microspheres at high repetition frequencies (*f*). These results offer a novel understanding of the photophysical processes of organic TADF materials and provide valuable guidance for the development of miniaturized lasers with specific functionalities.

## Results and Discussion

2,3,5,6-tetrakis (carbazol-9-yl)-1,4-dicyanobenzene (4CzTPN, Figure 1a and Figure S1) with broad emission centered at 520 nm (Figure 1b) was selected as model compound for the following reasons. (i) The short delayed fluorescence lifetime is considered to provide an efficient RISC process.<sup>[6b]</sup> (ii) The high photoluminescence quantum yield (PLQY) of 4CzTPN (71.4%, Figure S2), which is consistent with that in previous work,<sup>[5a]</sup> is promising to offer a large optical gain.<sup>[6b,7]</sup>

As the natural transition orbitals (NTOs) shown in Figure 1c, all the four carbazole units make nearly equal contributions to the hole wave function of the  $S_1$  state but only two of them contribute significantly to the first triplet ( $T_1$ ) state, while both of the  $T_1$  and  $S_1$  show similar electron NTOs concentrated on the central phenyl ring and cyano groups.

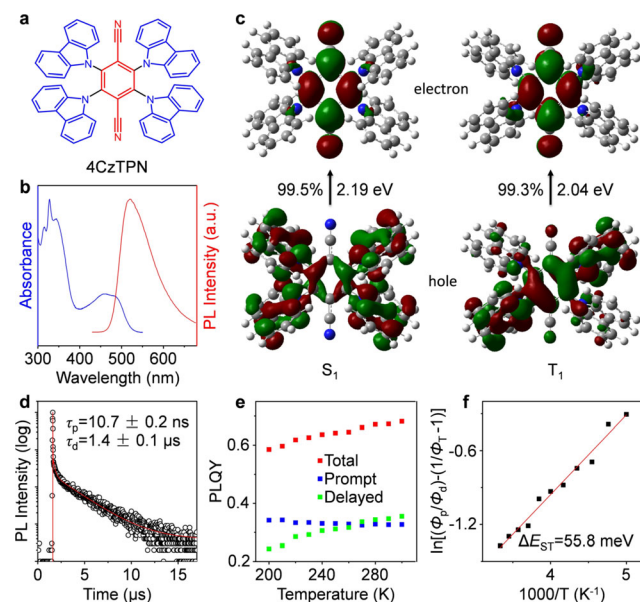


**Figure 1.** a) Chemical structure of 4CzTPN. b) UV/Vis absorption and PL spectra of degassed 4CzTPN solution (0.01 mM in toluene) at RT. c) Calculated hole and electron NTOs in 4CzTPN at optimized  $S_1$  and  $T_1$  geometries. d) PL decay profile of degassed 4CzTPN solution (0.01 mM in toluene) at RT. e) Temperature-dependent PLQYs for total, prompt and delayed components of a 3 wt% PS blend film. f) Berberan-Santos plot in the temperature range from 200 K to 300 K.

The separations of hole and electron densities result in typical charge-transfer features of the excited states. More importantly, the distinctly different transition nature can promote the spin-orbit coupling (SOC) between  $S_1$  and  $T_1$  states according to the El-Sayed rule, which would lead to a small  $S_1$ - $T_1$  energy gap ( $\Delta E_{ST}$ ) for the emergence of TADF. The photoluminescence (PL) decay curve of 4CzTPN in degassed solution shows a nanosecond-scale prompt component and a microsecond-scale delayed component (Figure 1d), which can be assigned to prompt fluorescence and delayed fluorescence, respectively. The short lifetime of the prompt component ( $10.7 \pm 0.2$  ns) implies a high radiative decay rate of the prompt fluorescence, which is promising for lasing because the lasing threshold is generally inversely proportional to the radiative decay rate.<sup>[6b]</sup> The lifetime of the delayed component ( $1.4 \pm 0.1$   $\mu$ s) is much shorter than that of most TADF materials (tens of microseconds to milliseconds),<sup>[8]</sup> indicating an efficient RISC process in 4CzTPN molecules.

The RISC process was investigated in depth with 4CzTPN molecule-doped polystyrene (PS) film, considering that atmospheric oxygen can be blocked by the PS matrix to maintain the TADF features of 4CzTPN (Figure S3 and S4).<sup>[9]</sup> The optimal concentration of 4CzTPN molecules in PS matrix was determined to be  $\approx 3$  wt% for a balance between RISC efficiency and ASE threshold (Figure S5). Figure 1e shows the temperature dependence of the PLQYs for the total, prompt, and delayed components of a 3 wt% PS blend film (detailed data are summarized in Table S1). The prompt component increases as temperature decreases, suggesting suppression of the non-radiative decay from  $S_1$ . Conversely, the delayed component and total PLQY monotonically decrease as the temperature decreases because RISC becomes the rate-determining step. According to the Berberan-Santos plot,<sup>[10]</sup> the triplet formation efficiency ( $\Phi_T$ ) and activation energy  $\Delta E_{ST}$  were estimated to be 0.6 and 55.8 meV (Figure S6 and Figure 1f), respectively. The large  $\Phi_T$  indicates that the majority of radiative singlet excitons are transformed into non-radiative triplet excitons under optical excitation, leading to severe energy losses. Fortunately, the triplet excitons might be harvested and converted back to radiative singlet excitons through RISC processes owing to the small  $\Delta E_{ST}$ . Therefore, the rate constant of the RISC process ( $k_{RISC}$ ) is critical to the evaluation of the TADF efficiency. Here,  $k_{RISC}$  was calculated to be  $2.2 \times 10^6$  s<sup>-1</sup> (see details in Section S1), which is much larger than that of most TADF materials in previous reports,<sup>[5c,8]</sup> implying a good triplet-harvesting ability.

The efficient TADF processes may significantly contribute to singlet lasing due to the energy harvested from triplet states. 4CzTPN molecules were introduced into polymeric microspheres through an emulsion-solvent-evaporation method.<sup>[11]</sup> A well-mixed 4CzTPN/PS/ $CH_2Cl_2$  solution was added to a cetyltrimethylammonium bromide (CTAB) aqueous solution. Under vigorous stirring, an oil-in-water emulsion was formed (Figure S7). The hydrophobic 4CzTPN/PS/ $CH_2Cl_2$  solution was encapsulated in the hydrophobic interior of CTAB micelles. After the complete evaporation of the  $CH_2Cl_2$  solvent, the PS molecules aggregated into low-crystallinity microspheres owing to the isotropic interfacial



tension (Figure S8). The obtained microspheres have perfect circular boundaries and ultrasmooth surfaces with polydispersity below 10% (Figure S9 and S10),<sup>[12]</sup> which are favorable for WGM resonance that tightly confines photons by means of continuous total internal reflection (Figure S11).<sup>[13]</sup> All the fabricated microspheres show homogeneous green-yellow fluorescence under ultraviolet (UV) light (330–380 nm) excitation (Figure 2a), indicating the uniform dispersion of 4CzTPN molecules in the PS matrix.

When a 4CzTPN-doped microsphere was locally excited with a focused pulsed laser beam (400 nm,  $\approx 200$  fs) in a homemade microphotoluminescence system (Figure S12), a bright rim at the outer boundary of the microsphere was observed (Figure 2b). At low pump fluence, the emission spectrum of the doped microstructure exhibits a series of cavity-mode peaks with green-yellow emission centered at  $\approx 520$  nm (Figure 2c), which is in good accordance with the spontaneous emission in the blend film (Figure S3). With increasing pump fluence, the PL intensity at approximately 563 nm is dramatically amplified as a set of sharp peaks, manifesting lasing action from the 4CzTPN-doped microsphere. Moreover, the emission at 563 nm is strongly linearly polarized (Figure 2c, inset), which shows the typical polarization characteristic of a laser.<sup>[14]</sup>

In Figure 2d, the emission energy (obtained by integrating corresponding laser peak) exhibits an S-shape nonlinear dependence on the pump fluence. Below  $88 \mu\text{J cm}^{-2}$ , the emission energies are well-fitted to the power law  $x^p$  with  $p = 0.40$ ,<sup>[15]</sup> showing a sublinear regime where bimolecular quenching (exciton-exciton annihilation) dominates. Super-linear relationship is found above threshold with  $p = 5.11$ , clearly showing a lasing process.<sup>[16]</sup> The flat curve with  $p = 0.55$  at high pump densities ( $> 128 \mu\text{J cm}^{-2}$ ) indicates the saturation of the gain media. The full-width-at-half-maximum

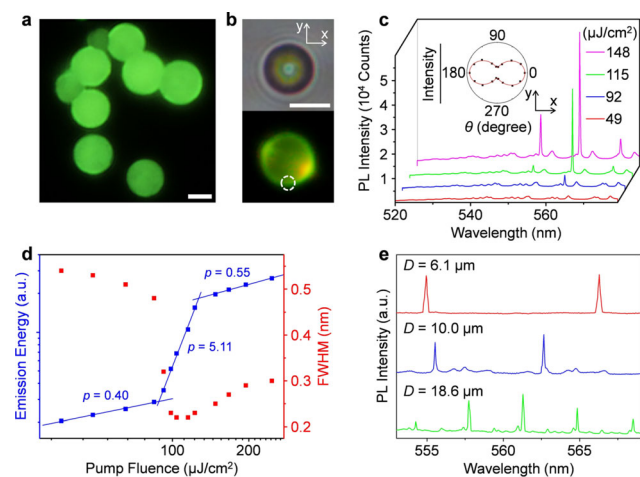


**Figure 2.** a) PL image of 4CzTPN microspheres. Scale bar = 5  $\mu\text{m}$ . b) Bright-field and PL images of an identical microsphere excited with a pulsed laser. Scale bar = 5  $\mu\text{m}$ . c) PL spectra of the doped microsphere under different pump fluences. Inset: Polar plot of lasing intensities collected from the marked area (white circle) in (b). d) Plots of emission energy and FWHM as a function of pump fluence. e) Lasing spectra of 4CzTPN-doped microspheres with different diameters.

(FWHM) at 563 nm dramatically narrows down to  $\approx 0.21$  nm when pump fluence exceeds the lasing threshold, implying a sharp increase of temporal coherence. The lasing spectra of 4CzTPN-doped microspheres with different diameters ( $D$ ) are presented in Figure 2e. The mode spacing ( $\Delta\lambda$ ) decreases with increasing  $D$  of the microspheres. The linear relationship of  $\lambda^2/\Delta\lambda$  versus  $D$  of the microspheres at  $\lambda = 562$  nm indicates that the PL modulation originates from the WGM-type cavity resonance (Figure S13). The calculated  $Q$  factors are on the order of  $10^3$  (Figure S14), which is pretty high for organic resonators. Moreover, we recorded the input-output intensity profiles of 30 different microspheres, and all the samples showed obviously nonlinear amplification behavior with thresholds of  $84\text{--}95 \mu\text{J cm}^{-2}$  (Figure S15), validating the lasing performance of different microspheres.

The lasing mechanism of the 4CzTPN-doped microspheres was explored with nanosecond transient absorption (ns-TA) spectroscopy. As shown in Figure 3a, following selective photoexcitation at 355 nm, the 4CzTPN-doped microspheres exhibit two negative bands at approximately 480 nm and 560 nm and a positive band at 530 nm. The negative signal at approximately 480 nm can be assigned to ground state bleaching according to the steady-state absorption spectrum shown in Figure S3. The other strong negative signal with the main peak close to the fluorescence emission of the 4CzTPN microspheres is ascribed to stimulated emission with a decay lifetime of  $1.5 \pm 0.1 \mu\text{s}$  (Figure 3b, up), which is consistent with the lifetime of the delayed fluorescence. Meanwhile, the positive absorption band is attributed to the  $T_1 \rightarrow T_n$  excited absorption of the 4CzTPN molecules.<sup>[17]</sup> The lifetime of the triplet state is  $1.6 \pm 0.1 \mu\text{s}$ , obtained by fitting the time trace of the ESA band at 530 nm (Figure 3b, bottom), which is almost the same as that of the delayed fluorescence. The transient absorption spectroscopy strongly indicates the existence of an RISC process in

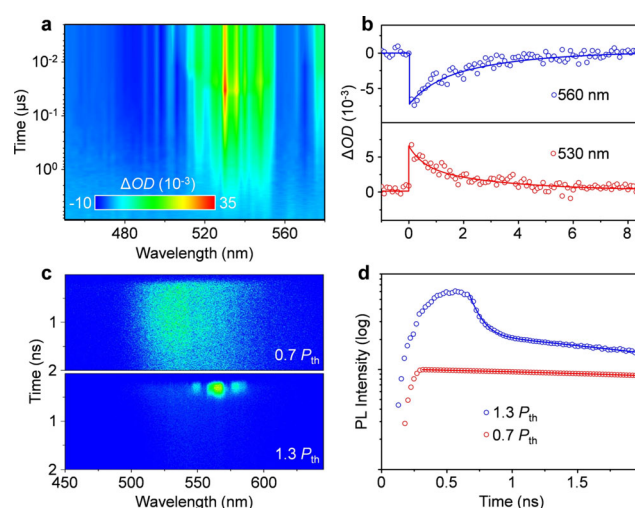


**Figure 3.** a) ns-TA spectra of 3 wt% 4CzTPN-doped microspheres excited with a pulsed 355 nm ns laser. b) Transient decay profiles with solid lines presenting the global fits at 560 nm and 530 nm. c) Streak camera images of an identical 4CzTPN-doped microsphere at pump densities of  $0.7 P_{\text{th}}$  (top) and  $1.3 P_{\text{th}}$  (bottom). d) Corresponding TRPL decay curves monitored at 566 nm.

4CzTPN molecules. More importantly, the small overlap between the ESA spectra and the gain region leads to negligible triplet absorption losses, indicating the presence of a large gain window at the lasing wavelength.

Time-resolved PL (TRPL) measurements were performed to clarify the lasing process of the microspheres. Figure 3c shows two streak camera images of an identical microsphere obtained under different excitation densities. A wide emission band with a long decay time is observed when the microsphere is excited by an excitation intensity below the lasing threshold ( $0.7P_{th}$ ). In contrast, narrow emission peaks with short decay times appear in the range of 540–580 nm when the excitation intensity is  $1.3P_{th}$ . The significant difference between the two images clearly demonstrates the generation of lasing above the threshold. Figure 3d shows TRPL decay curves spanning from spontaneous emission to stimulated emission. Below the lasing threshold ( $0.7P_{th}$ ), the PL mono-exponentially decays with a lifetime of approximately 10 ns, which corresponds to the lifetime of the prompt fluorescence (Figure S4). When the pump fluence exceeds the lasing threshold ( $1.3P_{th}$ ), a very fast time decay ( $\approx 92$  ps) dominates the kinetic process, signifying the occurrence of stimulated emission in the microsphere. Notably, the rise time is approximately 500 ps at  $1.3P_{th}$ , which is much longer than that of typical organic gain materials.<sup>[18]</sup> The long rise time can be attributed to the involvement of regenerated singlet excitons, which slows down the establishment of population inversion.

A schematic diagram showing the RISC-boosted lasing mechanism based on the above discussions is shown in Figure 4a. Upon optical excitation, 4CzTPN molecules undergo a transition from  $S_0$  to the excited singlet states and subsequently cool fast to the bottom of  $S_1$  (2.19 eV, Figure 1c). Two major pathways play a role in the deexcitation of the singlet state: radiative decay to the ground state and intersystem crossing to generate triplet excitons; the latter impedes the population accumulation in  $S_1$ . Benefiting from an efficient RISC process, most triplet excitons are converted to singlet excitons, which not only reduces the triplet accumulation in  $T_1$  (2.04 eV, Figure 1c) but also promotes the achievement of population inversion in  $S_1$ . Because RISC is an endothermic process that can be effectively activated at high temperatures, we expect that an increase in the temperature will increase the number of regenerated singlet excitons and thereby boost the lasing action in the 4CzTPN-doped microspheres.

Exactly, this is what we observed in the experiments. As shown in Figure 4b, the 4CzTPN-doped microsphere presents excellent lasing performance over a wide range of temperatures due to the strong cavity effect of the spherical morphology. Surprisingly, the lasing intensity gradually increases with the temperature increasing from 100 to 310 K (defined as forward direction in Figure 4c), which is in sharp contrast with the decreased lasing intensity at elevated temperatures in previous reports.<sup>[19]</sup> Meanwhile, the lasing intensity decreases with the temperature decreasing back from 310 to 100 K (the backward direction in Figure 4c), which is in accordance with the results in the forward direction. This exceptional performance can be reasonably

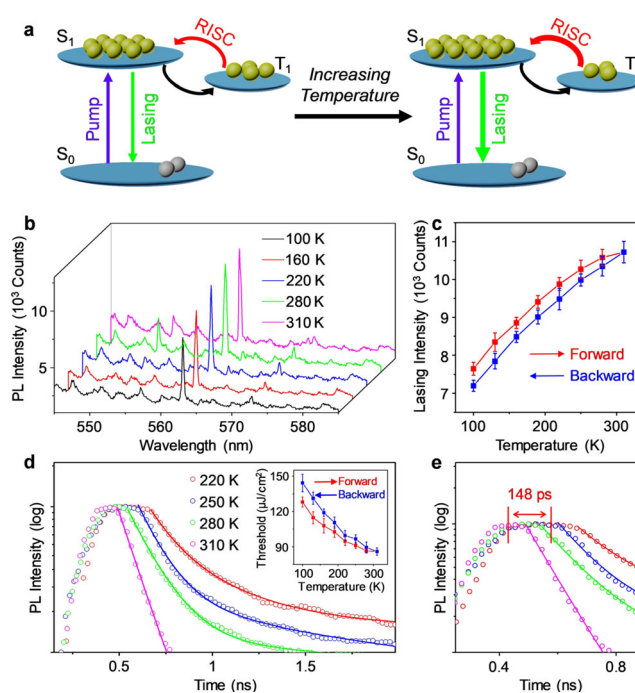


**Figure 4.** a) Schematic illustration of the triplet-harvesting lasing process. b) Temperature-dependent lasing spectra of an isolated 4CzTPN-doped microsphere. c) Plots of the lasing intensity of the microsphere versus temperature in forward and backward sweeps. Error bars represent the standard deviation of five representative measurements. d) Temperature-dependent TRPL decay curves monitored at lasing wavelength. Inset: temperature-dependent thresholds of an identical 4CzTPN-doped microsphere in sweeps. Error bars represent the standard deviation of five representative measurements. e) Magnification of the TRPL decay curves in (d) around the peak intensities. For (b)–(e), the pump fluences were fixed at  $1.7P_{th}$ .

ascribed to the involvement of regenerated singlet excitons in the stimulated emission process rather than the influence of PS matrix (Figure S16).<sup>[20]</sup> The rising temperature gradually accelerates the upconversion from  $T_1$  to  $S_1$ , which increases the number of regenerated singlet excitons and thereby results in thermally activated lasing. The microspheres serve as high-quality WGM resonators for laser oscillation, and more importantly, the uniform dispersion of 4CzTPN molecules in the microspheres prevents the aggregation-caused quenching effect that limits the RISC efficiency in solid-state materials, promoting the conversion from triplets to singlets. The difference of lasing intensities between the forward and backward directions is ascribed to the slight decrease of PLQY of gain media under intense excitation.

As a comparison, 4CzTPN single-crystalline microplates were studied; although these microplates can also serve as high-quality WGM cavities and provide sufficient feedback to support lasing (Figure S17), the strong  $\pi$ - $\pi$  interaction resulting from the dense molecular packing promotes non-radiative relaxation of the triplet states, leading to severe suppression of RISC processes. The suppression of the RISC processes results in a negligible number of regenerated singlet excitons for stimulated emission, and therefore, the lasing intensities of 4CzTPN microplates decrease with increasing temperature (Figure S18). Hence, the uniform dispersion of 4CzTPN



molecules in the spherical microcavities, which ensures an efficient RISC process in solid-state materials,<sup>[21]</sup> is essential to experimentally achieve RISC-boosted lasing.

As shown in Figure 4d, the lifetime of the stimulated emission in 4CzTPN-doped microspheres decreases with increasing temperature, demonstrating an acceleration of the depletion of the excited-state population. This phenomenon is similar to the power dependence of the lifetime observed in previous works,<sup>[22]</sup> where the increased exciton density with pump fluence accelerates the relaxation process and therefore results in a decreased lifetime. Considering that the pump fluence was fixed, the temperature-dependent lifetime of the stimulated emission is mainly attributed to the increased number of regenerated singlet excitons through the thermally promoted triplet-to-singlet upconversion, which decreases the threshold pump density as the temperature increases (Figure 4d, inset). Simultaneously, the PL shows a shorter rise time than that at lower temperature (Figure 4e and Table S2), implying that the establishment of population inversion was promoted by upconverted energy from triplets.

The thermally activated lasing process is further investigated by clarifying the pathway of triplet excitons to singlet states. In Figure S19, the energy level of the lowest charge-transfer triplet (<sup>3</sup>CT) state is lower than that of the lowest charge-transfer singlet (<sup>1</sup>CT) state with  $\Delta E_{ST}$  of 0.15 eV and SOC matrix element value of  $0.44 \text{ cm}^{-1}$ , which is attributed to the different transition nature of  $S_1$  and  $T_1$  states (Figure 1c). However, the relatively large energy gap (0.29 eV) leads to a weak vibronic coupling between <sup>3</sup>CT and the locally-excited triplet (<sup>3</sup>LE) state, which hinders the occurrence of RISC processes through the intermediate <sup>3</sup>LE state by vibronic coupling.<sup>[20]</sup> Therefore, the real RISC pathway in 4CzTPN should be the direct upconversion process from <sup>3</sup>CT to <sup>1</sup>CT state. All these experimental results clearly demonstrate that the lasing process in the microspheres has been effectively thermally activated through the <sup>3</sup>CT-<sup>1</sup>CT upconversion processes.

The triplet-harvesting RISC process is considered to overcome the triplet losses under successive excitation, which is the main stumbling block to achieve organic continuous-wave lasers.<sup>[23]</sup> When a microsphere was locally excited with a pulsed laser (343 nm, 450 fs,  $f$  of 0.025 MHz), a series of sharp peaks were found in the collected PL spectra taken from the edge of the microsphere (Figure 5a). With increasing pump fluence, the PL intensity in the gain region was dramatically amplified, manifesting lasing action from the dye-doped microsphere. The corresponding dependence of the emission energy on pump fluence showed a nonlinear behavior at the threshold of  $88 \mu\text{J cm}^{-2}$ , accompanied with decreasing FWHM down to 0.2 nm above the threshold (Figure 5b).

The lasing features of 4CzTPN-doped microspheres were investigated in depth in a wide range of  $f$ . With increasing  $f$  from 0.025 MHz to 0.5 MHz, the lasing thresholds decrease gradually from  $88 \pm 1.5 \mu\text{J cm}^{-2}$  to  $73 \pm 2.4 \mu\text{J cm}^{-2}$  (Figure 5c), signifying that the triplet losses have been minimized. Moreover, considering the delay fluorescence in 4CzTPN is sustained up to 15  $\mu\text{s}$  (Figure S4), pump pulses with a temporal spacing of  $1/(0.5 \text{ MHz}) = 2 \mu\text{s}$  should facilitate the harvest of

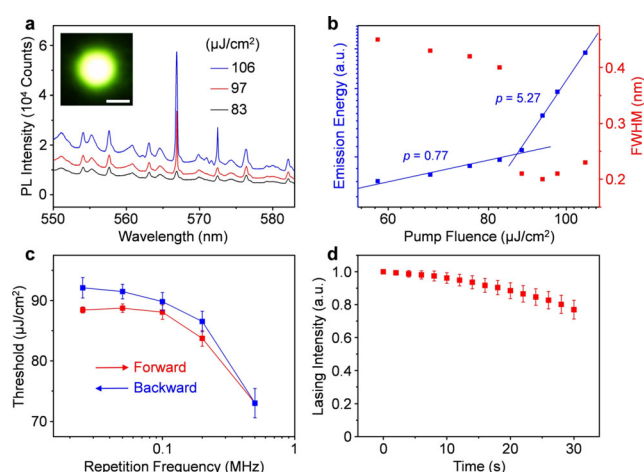


**Figure 5.** a) PL spectra of the doped microsphere under different pump fluences with  $f = 0.025$  MHz. Inset: PL image of the microsphere above lasing threshold. Scale bar =  $10 \mu\text{m}$ . b) Plots of emission energy and FWHM as a function of pump fluence with  $f = 0.025$  MHz. c) Plots of lasing thresholds of an identical 4CzTPN microsphere versus  $f$  in forward and backward sweeps. d) Shot-dependent lasing intensity of 3 wt% 4CzTPN doped microspheres. The pump fluence (with  $f = 0.5$  MHz) was fixed at  $1.3 P_{th}$ . Error bars represent the standard deviation of five representative measurements.

triplet excitons through RISC process for stimulated emission in the high- $f$  regime. The operational stability, which is crucial to evaluate the quality of the microlasers, was evaluated by continuously exciting a single sphere. In Figure 5d, the sustained operation of 4CzTPN microspheres demonstrates that the optical losses caused by the accumulation of triplet excitons under successive excitation were partially overcome by the RISC processes, showing a real advantage of using the TADF compound towards organic continuous-wave lasers.

## Conclusion

In summary, we experimentally observed distinct RISC-boosted lasing in self-assembled organic microspheres with homogeneously distributed TADF molecules. In these composite microcavities, the RISC process continuously converts non-radiative triplet excitons to radiative singlet excitons, contributing to the population inversion in  $S_1$ . Thermally activated lasing was achieved in the 4CzTPN-doped microspheres, where RISC processes play a key role in harvesting the triplet excitons and reducing the triplet losses. On this basis, exceptional activation of stimulated emission was observed by thermally boosting the RISC process, showing a sharp contrast to 4CzTPN single crystals with negligible triplet-harvesting capability. Owing to the harvest of triplet excitons by RISC processes, lasing from the microspheres was achieved at high  $f$ . These results not only provide us with deep insights into the excited-state processes of TADF materials but also indicate a promising direction for developing organic photonic elements with desired functionalities.

## Acknowledgements

The authors thank Mingxing Chen (Analytical Instrumentation Center of Peking University) for the assistance of temperature-dependent experiments and Prof. Andong Xia for the helpful discussions. This work was supported financially by the Ministry of Science and Technology of China (Nos. 2017YFA0204502), the National Natural Science Foundation of China (Nos. 21773265, 21922307 and 21790364), and the Chinese Academy of Sciences (2014028).

## Conflict of interest

The authors declare no conflict of interest.

**Keywords:** organic lasers · reverse intersystem crossing · temperature-dependent lasing · thermally activated delayed fluorescence · triplet-harvesting

- [1] a) N. Tessler, G. J. Denton, R. H. Friend, *Nature* **1996**, *382*, 695–697; b) I. D. W. Samuel, G. A. Turnbull, *Chem. Rev.* **2007**, *107*, 1272–1295; c) A. J. C. Kuehne, M. C. Gather, *Chem. Rev.* **2016**, *116*, 12823–12864; d) S. W. Eaton, A. Fu, A. B. Wong, C.-Z. Ning, P. Yang, *Nat. Rev. Mater.* **2016**, *1*, 16028.
- [2] a) A. Rose, Z. Zhu, C. F. Madigan, T. M. Swager, V. Bulović, *Nature* **2005**, *434*, 876–879; b) M. C. Gather, S. H. Yun, *Nat. Photonics* **2011**, *5*, 406–410; c) J. Zhao, Y. Yan, Z. Gao, Y. Du, H. Dong, J. Yao, Y. S. Zhao, *Nat. Commun.* **2019**, *10*, 870; d) Z. Zhou, J. Zhao, Y. Du, K. Wang, J. Liang, Y. Yan, Y. S. Zhao, *Angew. Chem. Int. Ed.* **2020**, *59*, 11814–11818; *Angew. Chem.* **2020**, *132*, 11912–11916.
- [3] a) M. A. Baldo, R. J. Holmes, S. R. Forrest, *Phys. Rev. B* **2002**, *66*, 035321; b) Y. Zhang, S. R. Forrest, *Phys. Rev. B* **2011**, *84*, 241301; c) Y. Mi, Y. Zhong, Q. Zhang, X. Liu, *Adv. Opt. Mater.* **2019**, *7*, 1900544; d) P. Andrew, G. A. Turnbull, I. D. W. Samuel, W. L. Barnes, *Appl. Phys. Lett.* **2002**, *81*, 954–956.
- [4] M. Lehnhardt, T. Riedl, T. Weimann, W. Kowalsky, *Phys. Rev. B* **2010**, *81*, 165206.
- [5] a) H. Uoyama, K. Goushi, K. Shizu, H. Nomura, C. Adachi, *Nature* **2012**, *492*, 234–238; b) H. Wang, L. Xie, Q. Peng, L. Meng, Y. Wang, Y. Yi, P. Wang, *Adv. Mater.* **2014**, *26*, 5198–5204; c) Y. Tao, K. Yuan, T. Chen, P. Xu, H. Li, R. Chen, C. Zheng, L. Zhang, W. Huang, *Adv. Mater.* **2014**, *26*, 7931–7958; d) Y. Liu, C. Li, Z. Ren, S. Yan, M. R. Bryce, *Nat. Rev. Mater.* **2018**, *3*, 18020; e) X.-K. Chen, D. Kim, J.-L. Brédas, *Acc. Chem. Res.* **2018**, *51*, 2215–2224; f) K. Wu, T. Zhang, Z. Wang, L. Wang, L. Zhan, S. Gong, C. Zhong, Z.-H. Lu, S. Zhang, C. Yang, *J. Am. Chem. Soc.* **2018**, *140*, 8877–8886; g) M. Li, Y.-F. Wang, D. Zhang, L. Duan, C.-F. Chen, *Angew. Chem. Int. Ed.* **2020**, *59*, 3500–3504; *Angew. Chem.* **2020**, *132*, 3528–3532.
- [6] a) H. Nakanotani, T. Furukawa, T. Hosokai, T. Hatakeyama, C. Adachi, *Adv. Opt. Mater.* **2017**, *5*, 1700051; b) D.-H. Kim, A. D'Aléo, X.-K. Chen, A. D. S. Sandanayaka, D. Yao, L. Zhao, T. Komino, E. Zaborova, G. Canard, Y. Tsuchiya, E. Choi, J. W. Wu, F. Fages, J.-L. Brédas, J.-C. Ribierre, C. Adachi, *Nat. Photonics* **2018**, *12*, 98–104.
- [7] M. D. McGehee, R. Gupta, S. Veenstra, E. K. Miller, M. A. Díaz-García, A. J. Heeger, *Phys. Rev. B* **1998**, *58*, 7035–7039.
- [8] Z. Yang, Z. Mao, Z. Xie, Y. Zhang, S. Liu, J. Zhao, J. Xu, Z. Chi, M. P. Aldred, *Chem. Soc. Rev.* **2017**, *46*, 915–1016.
- [9] a) T. N. Singh-Rachford, J. Lott, C. Weder, F. N. Castellano, *J. Am. Chem. Soc.* **2009**, *131*, 12007–12014; b) A. Monguzzi, M. Mauri, M. Frigoli, J. Pedrini, R. Simonutti, C. Larpent, G. Vaccaro, M. Sassi, F. Meinardi, *J. Phys. Chem. Lett.* **2016**, *7*, 2779–2785.
- [10] M. N. Berberan-Santos, J. M. M. Garcia, *J. Am. Chem. Soc.* **1996**, *118*, 9391–9394.
- [11] C. Wei, S.-Y. Liu, C.-L. Zou, Y. Liu, J. Yao, Y. S. Zhao, *J. Am. Chem. Soc.* **2015**, *137*, 62–65.
- [12] D. Comoretto, *Organic and Hybrid Photonic Crystals*, Springer, Cham, **2015**.
- [13] a) V. D. Ta, R. Chen, H. D. Sun, *Adv. Mater.* **2012**, *24*, OP60–OP64; b) X. Wang, Q. Liao, Q. Kong, Y. Zhang, Z. Xu, X. Lu, H. Fu, *Angew. Chem. Int. Ed.* **2014**, *53*, 5863–5867; *Angew. Chem.* **2014**, *126*, 5973–5977; c) B. Tang, L. Sun, W. Zheng, H. Dong, B. Zhao, Q. Si, X. Wang, X. Jiang, A. Pan, L. Zhang, *Adv. Opt. Mater.* **2018**, *6*, 1800391; d) Y. Mi, B. Jin, L. Zhao, J. Chen, S. Zhang, J. Shi, Y. Zhong, W. Du, J. Zhang, Q. Zhang, T. Zhai, X. Liu, *Small* **2019**, *15*, 1901364.
- [14] Y. Zhang, S. Wang, S. Chen, Q. Zhang, X. Wang, X. Zhu, X. Zhang, X. Xu, T. Yang, M. He, X. Yang, Z. Li, X. Chen, M. Wu, Y. Lu, R. Ma, W. Lu, A. Pan, *Adv. Mater.* **2020**, *32*, 1808319.
- [15] S. Kéna-Cohen, S. R. Forrest, *Nat. Photonics* **2010**, *4*, 371–375.
- [16] a) Y. Yu, Z.-Z. Li, J.-J. Wu, G.-Q. Wei, Y.-C. Tao, M.-L. Pan, X.-D. Wang, L.-S. Liao, *ACS Photonics* **2019**, *6*, 1798–1803; b) J.-J. Wu, H. Gao, R. Lai, M.-P. Zhuo, J. Feng, X.-D. Wang, Y. Wu, L.-S. Liao, L. Jiang, *Matter* **2020**, *2*, 1233–1243; c) F. F. Xu, Y. J. Li, Y. Lv, H. Dong, X. Lin, K. Wang, J. Yao, Y. S. Zhao, *CCS Chem.* **2020**, *2*, 369–375.
- [17] T. Hosokai, H. Matsuzaki, A. Furube, K. Tokumaru, T. Tsutsui, H. Nakanotani, M. Yahiro, C. Adachi, *SID Symp. Dig. Tech. Pap.* **2016**, *47*, 786–789.
- [18] a) K. Kamada, K. Sasaki, H. Misawa, N. Kitamura, H. Masuhara, *Chem. Phys. Lett.* **1993**, *210*, 89–93; b) I. Gozhyk, M. Boudreau, H. R. Haghghi, N. Djellali, S. Forget, S. Chénais, C. Ulysse, A. Brosseau, R. Pansu, J.-F. Audibert, S. Gauvin, J. Zyss, M. Leblental, *Phys. Rev. B* **2015**, *92*, 214202.
- [19] a) V. G. Kozlov, V. Bulović, S. R. Forrest, *Appl. Phys. Lett.* **1997**, *71*, 2575–2577; b) C. Spiegelberg, N. Peyghambarian, B. Kippelen, *Appl. Phys. Lett.* **1999**, *75*, 748–750.
- [20] M. K. Etherington, J. Gibson, H. F. Higginbotham, T. J. Penfold, A. P. Monkman, *Nat. Commun.* **2016**, *7*, 13680.
- [21] J. Lee, N. Aizawa, M. Numata, C. Adachi, T. Yasuda, *Adv. Mater.* **2017**, *29*, 1604856.
- [22] a) J. C. Johnson, K. P. Knutsen, H. Yan, M. Law, Y. Zhang, P. Yang, R. J. Saykally, *Nano Lett.* **2004**, *4*, 197–204; b) H. Dong, C. Zhang, Y. Liu, Y. Yan, F. Hu, Y. S. Zhao, *Angew. Chem. Int. Ed.* **2018**, *57*, 3108–3112; *Angew. Chem.* **2018**, *130*, 3162–3166.
- [23] a) R. Bornemann, U. Lemmer, E. Thiel, *Opt. Lett.* **2006**, *31*, 1669; b) T. Rabe, K. Gerlach, T. Riedl, H.-H. Johannes, W. Kowalsky, J. Niederhofer, W. Gries, J. Wang, T. Weimann, P. Hinze, F. Galbrecht, U. Scherf, *Appl. Phys. Lett.* **2006**, *89*, 081115; c) A. S. D. Sandanayaka, T. Matsushima, F. Bencheikh, K. Yoshida, M. Inoue, T. Fujihara, K. Goushi, J.-C. Ribierre, C. Adachi, *Sci. Adv.* **2017**, *3*, e1602570.

Manuscript received: June 26, 2020

Revised manuscript received: July 29, 2020

Accepted manuscript online: August 13, 2020

Version of record online: ■ ■ ■ ■ ■ ■ ■ ■ ■ ■

## Research Articles

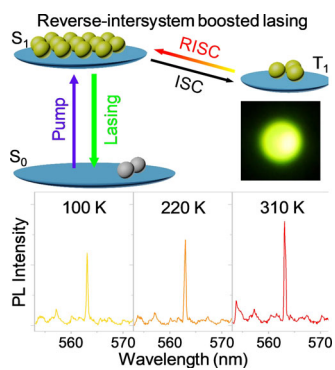


## Organic Lasers

Z. Zhou, C. Qiao, K. Wang, L. Wang,  
J. Liang, Q. Peng, Z. Wei, H. Dong,  
C. Zhang, Z. Shuai, Y. Yan,\*  
Y. S. Zhao\*



Experimentally Observed Reverse  
Intersystem Crossing-Boosted Lasing



Reverse intersystem crossing-boosted lasing was experimentally demonstrated in self-assembled microspheres with uniformly dispersed organic thermally activated delayed-fluorescence molecules. The lasing intensity increases with increasing temperature due to the involvement of regenerated singlets in population inversion, which provides a way to overcome triplet-related losses for high-performance organic lasers.

